

Received November 29, 2019, accepted December 6, 2019, date of publication December 13, 2019, date of current version December 26, 2019.

Digital Object Identifier 10.1109/ACCESS.2019.2958941

Patch-Based Nonlocal Adaptive Gradient Regularization for Image Restoration in Sensor Networks

MINGZHU SHI 

Tianjin Key Laboratory of Wireless Mobile Communications and Power Transmission, Tianjin Normal University, Tianjin 300387, China
College of Electronic and Communication Engineering, Tianjin Normal University, Tianjin 300387, China

e-mail: shimingzhu1@163.com

This work was supported by the National Natural Science Foundation of China under Grant 61501328.


ABSTRACT In this paper, we propose a novel patch-based adaptive nonlocal gradient regularization method for image restoration in sensor networks. It formulates the hyper-Laplacian distribution to regularize the global gradient distribution. The patch-based nonlocal gradient prior is utilized to regularize the nonlocal self-similarity of image gradients. Firstly, the L_0 -norm smoothing scheme is used innovatively as the preprocessing step to preserve strong edges, which are critical to improve the accuracy of clustering the similar image patches. Then, adaptive weights for each patches are developed from a set of clustered nonlocal self-similarity patches by learning the the expectation and variance for sparse gradient distribution at each pixel. Comparing with several recent state-of-the-art methods, experimental results show that the proposed method has better performance in alleviating block effects and preserving image details.

INDEX TERMS L_0 -norm regularization, image restoration, hyper-Laplacian, image priors.

I. INTRODUCTION

With the rapid development of wireless sensor networks, there is an increasing demand for the quality of signal transmission, especially for the two-dimensional images, which are inevitably degraded in the process of image acquisition, transmission and processing. Naturally, image restoration with the purpose of recovering a high quality original images plays an important role in mid-level and high-level image processing tasks [1], [2]. In the spatially invariant system, the imaging process is often formulated as a common model $\mathbf{y} = H\mathbf{x} + \mathbf{n}$. Here \mathbf{y} is the degraded image, \mathbf{x} is the desired image and \mathbf{n} is the additive Gaussian white noise with zero mean. H denotes the degraded process, which is the discrete point spread function (PSF) and usually modeled as a blurring matrix. The recovered results may be discontinuous because of observation errors, which lead to the high ill-posed problem. Thus, regularizing such ill-posed problem is critical to obtain a stable solution and produce a desire image.

In the maximum a posteriori (MAP) framework, the posterior of the recovered procedure often be modeled as $P(\mathbf{x} | \mathbf{y}, H) \propto P(\mathbf{y} | \mathbf{x}, H)P(\mathbf{x})$. Here, the likelihood $P(\mathbf{y} | \mathbf{x}, H)$

The associate editor coordinating the review of this manuscript and approving it for publication was Qilian Liang .

is usually specified as Gaussian distribution, which yields a well-known conditional probability density function

$$P(\mathbf{y} | \mathbf{x}, H) = N(\mathbf{y} | H\mathbf{x}, \sigma_n^2 \mathbf{I}) \propto \exp\left(-\frac{1}{2\sigma_n^2} \|\mathbf{y} - H\mathbf{x}\|_2^2\right), \quad (1)$$

where σ_n^2 is the noise variance and \mathbf{I} denotes an identity matrix. According to the Bayes rules, the corresponding object function can be modeled as

$$\hat{\mathbf{x}} = \arg \min_{\mathbf{x}} \left\{ \frac{\lambda}{2} \|\mathbf{y} - H\mathbf{x}\|_2^2 + \Phi(\mathbf{x}) \right\}, \quad (2)$$

where $\|\cdot\|_2$ is the Euclidean norm and the first term $\frac{\lambda}{2} \|\mathbf{y} - H\mathbf{x}\|_2^2$ denotes the energy-fidelity or data-fidelity term. $\Phi(\mathbf{x})$ is the regularization term that usually needs the image prior information to obtain the underlying solution. $\lambda > 0$ is the regularization parameter used to balance the fidelity term and regularization term. The PSF H is unknown in actual imaging cases, and the image restoration problem is still highly ill-posed even the blur kernel is known. It can be explained that the blur kernel is regarded as the low pass filter that tends to smooth the high frequency components, which leads to a loss of image details such as textures and edges. Therefore, developing an accurate image regularization method is critical to obtain the stable solution and

produce the high-quality recovered image. And the main purpose of this paper is developing appropriate image priors and adaptive spatial constraints.

A. RELATED WORKS

Many approaches have been developed for modeling and regularizing image priors. Some can be ascribed for image priors that exploit the statistics of natural image [3], others are based on the salient edges extracted from the image gradient domain [4]. Previous attempts in establishing image priors relied on modeling local pixel gradients with Laplacian distributions (total variation) [5], hyper-Laplacian distribution [6], [7], Gaussian mixture models [8], or generalized Gaussian distribution [9]. Recently, image priors have also been designed by formulating coefficients of the image in a transformed domains such as the discrete cosine transform domain and the discrete wavelet transform domain via scaled mixture of Gaussian priors [10]. The most basic idea of these works can be considered that images are sparsely represented in certain domains. In addition to the transform domain, the gradient domain is also widely used in image restoration problems as a typical spatial domain. The statistics and analysis of the images in the transform and the spatial domain show that images have self-similarity, scale in-variance, edge-dominant characteristics and high-dimensional heterogeneity. However, the high-dimensionality of the image makes it difficult to learn and optimize related prior knowledge from natural images. Obviously, the more appropriate the image priors and regularization schemes are, the more the natural information of the image can be better used to obtain high quality results.

Patch-based image priors have drawn more and more attention from experts to try various regularization schemes. Especially formulating the distribution of image patches has proven to get a stable solution [11], which mainly use the non-local self-similarity [12], [13], fields of experts [14], learned patch distribution [15]–[18]. Cho *et al.* [19] proposed a variational image restoration method that divided the image into square patches and used image priors to each patches independently. A typical non-local based variant total variation (NLTV) algorithm [20] assigns weights using the variation between any two pixels in a searching window. If they are not relevant, they will be assigned a small weight. However, the irrelevant contents can still influence the accuracy of algorithm. The popular BM3D [21] algorithm applies both two-dimensional and three-dimensional transform domains of the non-local self-similarity of image patches to achieve collaborative filtering. Using the non-local mean theory, Dong *et al.* [22] propose the non-local centralized sparse representation model to obtain the estimation of the sparse coding coefficients of the original image. By taking advantage of the non-local similarity of natural images, Liu *et al.* [23] formulate the sparsity of the image gradient with pixel-wise content-adaptive distributions to reflect the non-stationary nature of image statistics. Daniel and Weiss [24] propose the Expected Patch Log Likelihood (EPLL) method by using a

Gaussian mixture model (GMM) prior, which trains clean image patches to regularize degraded image patches. The GMM model has been proved to be more effective, popular and extendable to other sparsity constraints [25], [26]. Considering each patch has a patch classification step and a shrinkage step, Alban *et al.* [27] provide approximations and computational recipes to evaluate these two steps by embedding a generalized Gaussian mixture model into EPLL for an image with more than tens of thousands of patches. Assuming that the gradient distribution is spatial variant, Kang and Wu [28] propose an adaptive patched L_0 gradient minimization model that exploits the variational coefficient of roughly divided patches and sets the patch size adaptively. Clearly, developing appropriate patch-based adaptive gradient priors can improve the regularization of local information and obtain more satisfactory results.

B. OUR CONTRIBUTION

In this paper, we propose a patch-based adaptive nonlocal gradient regularization method for image restoration. The hyper-Laplacian distribution is formulated to regularize the global gradient distribution, and the nonlocal self-similarity of image gradients is utilized to regularize the patch-based nonlocal gradient prior. Especially, the L_0 -norm smoothing scheme is used innovatively as the preprocessing step to improve the accuracy of clustering the similar image patches. For spatial variation image prior, adaptive weights for each patches are developed from a set of clustered nonlocal self-similarity patches by learning the the expectation and variance for sparse gradient distribution at each pixel. Experimental results show that the proposed method can effectively alleviate block effects and preserve image details.

The main contributions of the proposed method can be summarized as follows:

- 1) proposing a novel patch-based adaptive nonlocal gradient regularization method that applies the statistical properties of the entire image and the self-similarity of image patches.
- 2) applying the L_0 -norm smoothing image as the preprocessed image to improve the accuracy of clustering the similar image patches. The K-Nearest-Neighbor (KNN) method is used to measure the similarity of image patches. KNN is calculated based on Euclidean distance by L_2 -norm to save computations.
- 3) developing patch-based adaptive weights from a set of nonlocal self-similarity patches by learning the expectation and variance for sparse gradient distribution at each pixel.

The reminder of this paper is organized as follows. Section II describes the image prior sparsity regularization scheme including the motivation of the proposed method, the novel image gradient prior and the adaptive patch-based non-local image prior. Section III introduces the proposed model and analyzes the numerical optimization algorithm. Experimental results are reported and discussed in Section IV, and Section V makes a conclusion.

II. IMAGE PRIOR SPASITY REGULARIZATION

A. MOTIVATION

Generally, the heavy-tailed distribution of the whole image gradient distribution is formulated as a unified hyper-Laplacian prior for the global image prior. However, the gradient distribution is spatially variant, it might be misleading because the statistic of natural images may not be stationary and the distribution of gradient data usually varies from one patch to another. Especially for the image with rich details, the regularization on regions with more textures or structures is usually emphasized that makes edges over-smoothed and leads to under-utilization of local information of the image. Many state-of-the-art algorithms can be attributed to using image priors obtained from statistical information of the natural image [6], [29]. However, some image information is still lost when noise is removed because of the preprocessing of the image. In the previous research [28], L_0 -norm is mainly used for resolving the image smoothing problem, in which image details are not important but edges are emphasized. Inspired, this paper considers preprocessing the image by the L_0 -norm to get strong edges and regularize the image gradient as the global constraint.

In many image restoration tasks, images to be recovered belong to some specific classes, such as faces, text, fingerprints, plants and buildings. Some images may have two or more classes because of multiple objects. Teodoro *et al.* [30] propose using patch-based image priors that are learned off-line from sets of clean images, and different image priors can be learned from sets containing just one class, or from sets containing two or more classes. This method is proven to effectively restore images with different structures. However, for a particular image restoration task, there may be several image classes in different regions of interest, which are hard to be extracted adaptively. In addition, both the selecting and the training of image sets are complicated and time consuming. Inspired by the nonlocal patch-based image priors and image classified training schemes, we mainly focus on utilizing the similar patches of the image itself that means using the self-similarity of image patches. For spatial constraints, we develop adaptive weights from a set of the searched nonlocal self-similarity patches by deriving the sparse gradient distribution at each pixel. The flow chart is shown in Figure 1, which briefly introduces the main schemes and steps of the proposed method. The image energy prior block is shown in Figure 1, and Eq.(1) in section I has given the specific formulation as an energy fidelity term $\|y - Hx\|_2^2 / 2\sigma_n^2$ for the whole image. In the following subsections, we will explain the proposed global image gradient regularization based on the hyper-laplacian distribution and the patch-based nonlocal regularization.

B. GLOBAL GRADIENT DISTRIBUTION PRIOR

The L_0 -norm regularization has been used for image smoothing by minimizing the image gradient. It can get better results for the piecewise constant image than the total variation

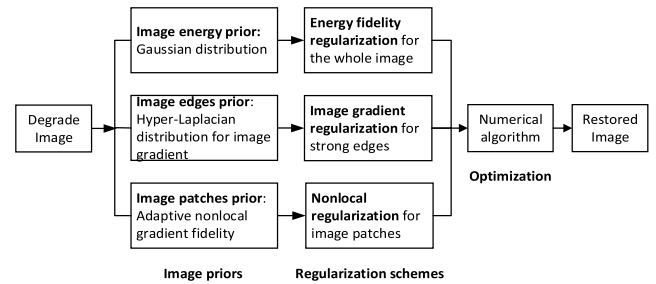


FIGURE 1. Flow chart of the proposed method.

method, which is the typical model using the L_1 -norm [31]. Xu *et al.* [32] propose an unnatural L_0 framework for single image deblurring by leveraging the L_0 sparse representation to greatly benefit kernel estimation and large-scale optimization. Based on the statistical characteristics of text images, Pan *et al.* [33] present a simple and effective L_0 -regularized prior from image intensity and gradient to estimate the blur kernel and latent images for text image deblurring. In single image deblurring. Therefore, the L_0 -norm can effectively protect strong edges in image denoising and smoothing tasks.

As mentioned above, the degraded image is obtained by the convolution operation of the original image and the blurred path. This is equivalent to image smoothing filter mathematically, which lead to a considerable amount of information lost. Thus, it is worth exploring whether the gradient distribution of the image is changed before and after degradation. Does the L_0 -norm image smoothing scheme also make the gradient distribution change? To explore the answer, we carry out experiments with various images and take a typical example for a natural image “flower”, whose gradient histograms in various cases are shown in Figure 2. Figure 2(a) is the original image that obeys the heavy-tailed distribution, as shown in Figure 2(b). Figure 2(c) is the image smoothed by the L_0 -norm, some details are smoothed but the strong edges are strengthened, which is reflected in the image gradient distribution histogram that the middle peak becomes sharper, as shown in Figure 2(d). Figure 2(e) is the blur image degraded by the random blur kernel in the top right. The gradient distribution histogram becomes narrower compared with that of the original image in Figure 2(b). This can be explained that some details-rich regions with the large pixel rang are smoothed out, and flat areas with small pixel rang occupy a relative larger proportion. Comparing Figure 2.(b) and (d), (f) and (h), it can be concluded that L_0 -norm smoothing scheme does not affect the gradient distribution of the image. Therefore, the L_0 -norm smoothing scheme is reasonable to be regarded as a global smoothing filter based on sparse strategy. Inspired, in this paper we use the L_0 -norm smoothing as the image preprocessing scheme, which can effectively smooth out the additional noise and preserve strong edges, and improve the clustering accuracy of similar patches.

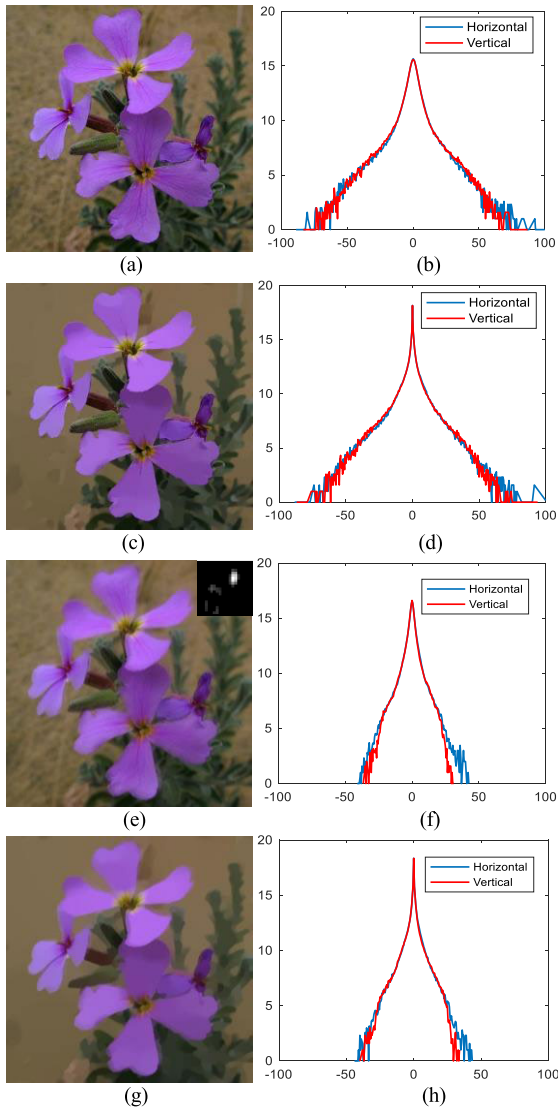


FIGURE 2. Images in different cases and corresponding gradient distributions: (a) Original image; (b) Gradient distribution of (a); (c) L_0 -norm smoothing image; (d) Gradient distribution of (c); (e) Degraded image by the blur kernel in the upper right of the image; (f) Gradient distribution of (e); (g) L_0 -norm smoothing for degrade image; (h) Gradient distribution of (g).

The global gradient distribution prior based on natural image statistics can be well modeled as the hyper-Laplacian distribution, and formulated by

$$P(\mathbf{x}) = \prod_i \exp(-|(\nabla \mathbf{x})_i|^p). \quad (3)$$

And its logarithm is

$$\Phi_{\text{global}}(\mathbf{x}) = -\log P(\mathbf{x}) \propto |(\nabla \mathbf{x})_i|^p. \quad (4)$$

According to the statistics of natural images, the norm p is usually ranged from 0.5 to 0.8. Moreover, if p is set to 1, it is the typical total variation norm; and if p is set to 2, it corresponds to the Gaussian function.

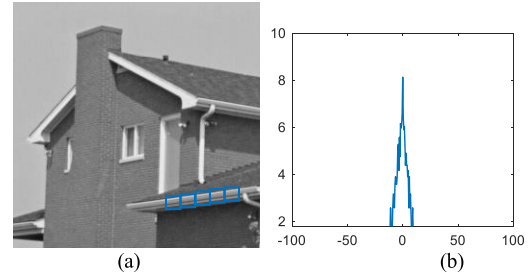


FIGURE 3. Image and gradient distributions of similar patches: (a) House image; (b) Gradient distribution of the sample image patches.

C. PATCH-BASED NONLOCAL GRADIENT PRIOR

Above hyper-laplacian gradient prior is formulated for the whole image, however, for the divided image patches, not each patch follows the same heavy-tailed distribution, especially for some flat patches that the gradient value tends to zero. The patch-based nonlocal gradient prior is proposed to regularize the information of image patches. More precisely speaking, the relevant image patches are similar to the current patch and are clustered by block matching scheme from the divided image patches. The patch-based nonlocal scheme is illustrated by the following Figure 3. In Figure 3(a), patches with the similar content marked by blue squares are collected as data samples to estimate the patch-based gradient distribution, and their gradient histogram is shown in Figure 3(b).

It is well known that the histogram curve does not represent the actual gradient value of all pixels but the statistical distribution. Pixels with large gradient values are not shown in the curve itself but located at the strong edges, and pixels with the gradient value of zero are located at the flat regions of the image. In order to establish an accurate gradient model at each pixel, the reference patch is located at the current pixel and similar patches are selected to form a set of divided image patches, and then the K-Nearest-Neighbor (KNN) algorithm is used to cluster the similar patches. There is a critical problem that cannot be ignored. Since the image is degraded and some details are lost, and the target image patch also becomes inaccurate. According to [34], the number of similar patches of an exemplar patch decay exponentially with the increase of the complex patches, which means that there may exist outliers within these KNN patches, especially for detailed patches. From this perspective, it can be better explained why the L_0 -norm image smoothing can help improve the extraction accuracy of similar patches. KNN has been used frequently in non-local methods to measure the similarity in the distance. By the L_2 -norm of intensity level of pixels in patches, it is defined as

$$d(i, j) = \left\| \mathbf{x}_i^0 - \mathbf{x}_j^0 \right\|_2^2. \quad (5)$$

Here, \mathbf{x}_i^0 and \mathbf{x}_j^0 denote the L_0 -norm smoothed image patches located at the pixel i and j , respectively. Block matching algorithm is applied for clustering the K most similar patches, whose positions are gathered in a set S_i . In order to provide

the adaptive spatial constraint and predict the actual gradient, the expectation m_i and variance σ_i of the gradient at pixel i from similar patches is calculated to learn the pixel distribution by

$$m_i = \frac{1}{|S_i|} \sum_{j \in S_i} D_j \mathbf{x}, D_j = \begin{bmatrix} D_j^h \\ D_j^v \end{bmatrix}$$

$$\sigma_i = \sqrt{\frac{1}{|S_i|} \sum_{j \in S_i} (D_j \mathbf{x} - m_i)^2} \quad (6)$$

Here, D denotes the directional difference operator, D_j^h and D_j^v denote the horizontal and vertical directions respectively.

Inspired by [23], the gradient difference between the target patch and similar patches is regularized by the total variation that is a typical L_1 -norm and has better performance in handling the directionality of the image. It can ensure the accuracy of prediction to avoid the disadvantage of the traditional total variation, which simply makes the regularization on the patch itself as zero. This deviation from the actual value often leads to staircase effects or block effects in the final recovered image. Hence, the patch-based spatial adaptive prior is formulated as

$$\Phi_{\text{nonlocal}}(\mathbf{x}) = \sum_i \left(\frac{\sqrt{2}}{\sigma_i^h} |D_i^h \mathbf{x} - m_i^h| + \frac{\sqrt{2}}{\sigma_i^v} |D_i^v \mathbf{x} - m_i^v| \right). \quad (7)$$

Here, it should be noted that ‘‘non-local’’ doesn’t express the same concept as the above definition ‘‘global’’ literally. $\Phi_{\text{nonlocal}}(\mathbf{x})$ means that uses the regularization information learned from the highly relevant image patches rather than local pixelwise, and thus is defined as the non-local regularization.

III. PROPOSED MODEL AND OPTIMIZATION

A. PROPOSED MODEL

The novelty of the proposed model is to make full use of the image statistical information. On the one hand, the whole distribution of the image gradient is used as the global constraint, and on the other hand, the self-similarity of similar image patches is used as the non-local adaptive gradient constraint. The framework of the proposed model is

$$\min_{\mathbf{x}} \left\{ \frac{\lambda}{2} \|\mathbf{y} - H\mathbf{x}\|_2^2 + \alpha \Phi_{\text{global}}(\mathbf{x}) + \Phi_{\text{nonlocal}}(\mathbf{x}) \right\}, \quad (8)$$

and the corresponding objective function can be formulated as

$$\min_{\mathbf{x}} \left\{ \frac{\lambda}{2} \|\mathbf{y} - H\mathbf{x}\|_2^2 + \alpha \left(|D^h \mathbf{x}|^p + |D^v \mathbf{x}|^p \right) + \sum_i \left(\frac{\sqrt{2}}{\sigma_i^h} |D_i^h \mathbf{x} - m_i^h| + \frac{\sqrt{2}}{\sigma_i^v} |D_i^v \mathbf{x} - m_i^v| \right) \right\}. \quad (9)$$

Here, λ depends on the noise level σ_n^2 that is often discussed together with the number and size of clustered patches [7]. It is a complex problem because the combination of three

norms, L_2 -norm, L_p -norm and L_1 -norm. The splitting variation method is applied to simply the problem and the function is rewritten as a constrained problem

$$\min_{\mathbf{x}} \left\{ \frac{\lambda}{2} \|\mathbf{y} - H\mathbf{x}\|_2^2 + \alpha \left(|\omega^h|^p + |\omega^v|^p \right) + \sum_i \left(\frac{\sqrt{2}}{\sigma_i^h} |\omega_i^h \mathbf{x} - m_i^h| + \frac{\sqrt{2}}{\sigma_i^v} |\omega_i^v \mathbf{x} - m_i^v| \right) \right\},$$

s.t. $\omega = D\mathbf{x}, \omega_i = D_i \mathbf{x}.$ (10)

The augmented Lagrangian method is used to transform it into an unconstrained problem and helps to avoid the ill-conditioning by implanting penalty terms [35]. The augmented Lagrangian is formulated as

$$L_A(\mathbf{x}, \mathbf{w}^h, \mathbf{w}^v) = \frac{\lambda}{2} \|\mathbf{y} - H\mathbf{x}\|_2^2 + \alpha \left(|\mathbf{w}^h|^p + |\mathbf{w}^v|^p \right) + \sum_i \left(\frac{\sqrt{2}}{\sigma_i^h} |\mathbf{w}_i^h \mathbf{x} - m_i^h| + \frac{\sqrt{2}}{\sigma_i^v} |\mathbf{w}_i^v \mathbf{x} - m_i^v| \right) + \frac{\beta}{2} \left(\|\mathbf{w}^h - D^h \mathbf{x}\|^2 + \|\mathbf{w}^v - D^v \mathbf{x}\|^2 \right) - \gamma^h (\mathbf{w}^h - D^h \mathbf{x}) - \gamma^v (\mathbf{w}^v - D^v \mathbf{x}), \quad (11)$$

where $\mathbf{w}^h = D^h \mathbf{x}, \mathbf{w}^v = D^v \mathbf{x}, \mathbf{w}_i^h = D_i^h \mathbf{x}$ and $\mathbf{w}_i^v = D_i^v \mathbf{x}$ are the auxiliary variables introduced. α and β are the regularization parameter for quadratic penalty terms $\|\mathbf{w} - D\mathbf{x}\|^2$. γ^h and γ^v are the Lagrangian multipliers for the constraint $(\mathbf{w} - D\mathbf{x})$. The problem in Eq.(11) is decomposed into three subproblems, which are simplified and resolved iteratively as

$$\begin{cases} (\mathbf{x}_{k+1}, \mathbf{w}_{k+1}^h, \mathbf{w}_{k+1}^v) \leftarrow \min_{\mathbf{x}, \mathbf{w}^h, \mathbf{w}^v} L_A(\mathbf{x}, \mathbf{w}^h, \mathbf{w}^v) \\ \gamma_{k+1}^h \leftarrow \gamma_k^h - \beta(\mathbf{w}_{k+1}^h - D^h \mathbf{x}_{k+1}) \\ \gamma_{k+1}^v \leftarrow \gamma_k^v - \beta(\mathbf{w}_{k+1}^v - D^v \mathbf{x}_{k+1}). \end{cases} \quad (12)$$

Here, k represents the number of iterations, and the alternating direction minimization method (ADMM) is adopted to solve above subproblems in Eq.(12) because of the good performance in terms of convergence.

B. OPTIMIZATION

With the fixed the norm p , an iterative optimization scheme is proposed to update \mathbf{w} and \mathbf{x} .

1) UPDATING \mathbf{x}

Given \mathbf{w}^h and \mathbf{w}^v , the problem can be rewritten as

$$\min_{\mathbf{x}} \frac{\lambda}{2} \|\mathbf{y} - H\mathbf{x}\|_2^2 + \frac{\beta}{2} \left(\left\| D^h \mathbf{x} - \mathbf{w}^h + \frac{\gamma^h}{\beta} \right\|^2 + \left\| D^v \mathbf{x} - \mathbf{w}^v + \frac{\gamma^v}{\beta} \right\|^2 \right). \quad (13)$$

It is a typical quadratic problem and has the closed-form solution

$$\mathbf{x} = \left[H^T H + \frac{\beta}{\lambda} D^T D \right]^{-1} \left[H^T \mathbf{y} + \frac{\beta}{\lambda} D^T \left(\mathbf{w} - \frac{\gamma}{\beta} \right) \right]. \quad (14)$$

Here, h and v are omitted to simplify the expression. For deconvolution, the degradation matrix H is factorized as a diagonal matrix by the two-dimensional discrete Fourier transform on the point spread function H . The coefficient matrix in Eq.(14) is always non-singular and should obey the standard assumption $N(H) \cap N(D) = 0$ to ensure the non-singularity. Here, $N(D)$ denotes the null space of a matrix. Obviously, with the periodic boundary condition of f , both $H^T H$ and $D^T D$ are block circulant matrix with circulant blocks (BCCB), and the $H^T H + \beta D^T D / \lambda$ can obtain its decomposed eigenvalues and is diagonalized by the two-dimension discrete Fourier transform, which only needs to calculate once. The BCCB matrix in Eq.(14) can be efficiently solved by the fast Fourier transform (FFT), and we get

$$\mathbf{x} = F^{-1} \left(\frac{F^*(D) \circ F \left(\mathbf{w} - \frac{\gamma}{\beta} \right) + \frac{\lambda}{\beta} F^*(H) \circ F(\mathbf{y})}{F^*(D) \circ F(D) + \frac{\lambda}{\beta} F^*(H) \circ F(H)} \right), \quad (15)$$

where F and F^{-1} represent the Fourier transform and the inverse Fourier transform respectively, $*$ denote the complex conjugate, \circ denotes the entry-wise multiplication. This scheme can reduce the computation cost to be $O(n \log n)$, where n denotes the number of pixels.

2) UPDATING \mathbf{w}^h AND \mathbf{w}^v

According to the Eq.(11) and (12), given \mathbf{x} , \mathbf{w}^h and \mathbf{w}^v are updated by following form

$$\min_{\mathbf{w}^h} \alpha \left| \mathbf{w}^h \right|^p + \sum_i \left(\frac{\sqrt{2}}{\sigma_i^h} \left| \mathbf{w}_i^h \mathbf{x} - m_i^h \right| \right) + \frac{\beta}{2} \left(\left\| \mathbf{w}^h - D^h \mathbf{x} - \frac{\gamma^h}{\beta} \right\|^2 \right) \quad (16)$$

and

$$\min_{\mathbf{w}^v} \alpha \left| \mathbf{w}^v \right|^p + \sum_i \left(\frac{\sqrt{2}}{\sigma_i^v} \left| \mathbf{w}_i^v \mathbf{x} - m_i^v \right| \right) + \frac{\beta}{2} \left(\left\| \mathbf{w}^v - D^v \mathbf{x} - \frac{\gamma^v}{\beta} \right\|^2 \right). \quad (17)$$

The above two subproblems can be solved by the generalized iterative shrinkage algorithm(GISA)[36].

Now the whole algorithm can be formally summarized as follows

IV. EXPERIMENTAL RESULTS

A. PARAMETER SETTING

We selected nine natural images as experimental image. Specially, for the global regularization, the hyper-laplacian

TABLE 1. Patch size testing (Lena-denoising results).

Patch size	5×5	9×9	13×13	17×17	25×25	255×255
PSNR	30.24	30.17	30.11	30.06	29.89	29.72



FIGURE 4. Test images: from left and right, from up and down, numbered from #1 to #9.

parameter p is determined from a large number of image statistics and is set to 0.5 based on research experience. We use the peak signal-to-noise ratio (PSNR) to evaluate the performance of the proposed patch-based nonlocal adaptive gradient regularization method.

In order to determine the most appropriate patch size, we test various sizes as 5×5 , 9×9 , 13×13 , 17×17 , 25×25 , and the whole image 255×255 . Results of the typical denoising experiments for the image ‘‘Lena’’ are list in table 1, it can be found that the smaller and the finer the size is, the better the evaluation value is obtained.

Both the patch size and the number of similar patches depend on the noise level, which also determines the value of the regularization parameter λ . [7] has provided the reference range of values, in this paper we set the noise standard deviation $\sigma_n = 20$ and $\lambda = 0.0025$, the patch size is 5×5 and the search window size is 32×32 . For each patch, number of the nearest neighbor patches N is set to 25. The exemplar patches are chosen along row and column directions every 5 pixels. The value of α controls the weight of the gradient regularization, here we set is as 0.005. The auxiliary parameters are set to $\beta = 0.012$ and $\gamma = 0.008$.

B. IMAGE RESTORATION RESULTS

In experiments, we use several common images to test the performance of the proposed method, as shown in Figure 4.

Different convolution matrices H in eq.(1) represent different tasks, which is essential in image transmission in sensor networks [37]. When H represent the identity matrix \mathbf{I} , it corresponds to the image denoising. When H is a diagonal

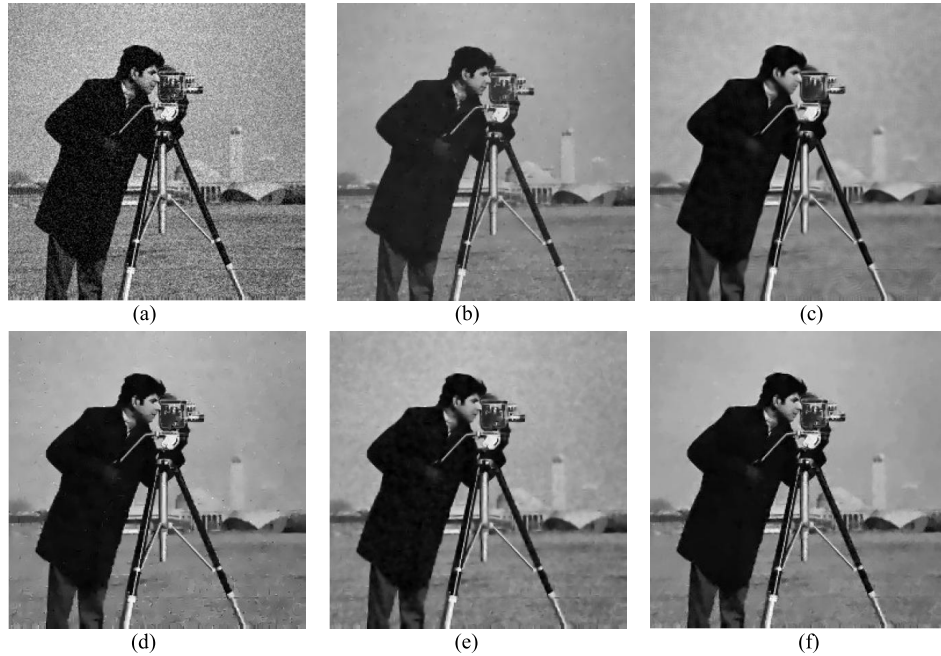


FIGURE 5. Comparison for image denoising methods of the noisy Cameraman at $\sigma = 20$: (a) Degrade image; (b) DnCNN [5], PSNR = 30.08dB; (c) FID-HL [6], PSNR = 29.33dB; (d) NLTV [20], PSNR = 29.80dB; (e) NGS [23], PSNR = 29.69dB; (f) Proposed method, PSNR = 30.11dB.

TABLE 2. Image denoising results of compared methods in PSNR(dB).

Method	σ_n	Images (#)								
		1	2	3	4	5	6	7	8	9
DnCNN	10	34.65	33.64	32.61	33.42	32.33	31.24	34.81	34.22	32.95
FID-HL		33.21	32.15	32.88	33.72	31.87	31.46	34.55	32.86	32.76
NLTV		33.63	32.91	33.48	34.45	32.62	31.87	34.86	33.12	33.17
NGS		34.43	33.64	33.84	34.76	32.97	32.24	35.62	33.88	33.64
Proposed		34.72	34.11	34.35	35.02	33.45	32.61	36.21	34.43	34.12
DnCNN	20	31.40	29.47	30.08	32.13	29.43	29.21	32.67	31.03	29.84
FID-HL		29.71	28.19	29.33	31.51	28.61	28.49	31.71	31.32	28.97
NLTV		30.35	28.74	29.84	31.84	29.02	28.71	32.46	31.73	29.41
NGS		30.65	29.52	29.79	32.12	29.41	29.04	33.12	32.26	30.02
Proposed		31.03	30.07	30.11	32.43	29.97	29.38	33.68	32.81	30.46
DnCNN	50	27.14	26.06	26.03	26.87	26.48	26.20	29.02	27.20	24.62
FID-HL		25.32	24.11	24.83	26.62	25.34	25.24	27.05	25.96	24.21
NLTV		25.47	24.67	25.04	26.68	25.61	25.57	27.67	26.61	24.27
NGS		26.15	25.12	25.19	27.14	25.82	25.86	28.47	27.65	24.65
Proposed		26.42	25.76	25.72	27.63	26.30	26.26	28.73	27.91	24.81

matrix with entries 0 or 1, it corresponds to the image inpainting. For image deblurring, we consider it as an random motion blur kernel.

1) IMAGE DENOISING

In image denoising, we compare the proposed method with several state-of-the-art methods, DnCNN [3], FID-HL [6], NLTV [20] and NGS [23]. The typical example on the image *Cameraman* is shown in Figure 5, Figure 5(a) is the noisy image degraded by the Gaussian noise with the standard deviation $\sigma = 20$. Figure 5(b) shows the result of the DnCNN method based on the convolutional neural network that uses an end-to-end trainable deep CNN for Gaussian denoising. It can not only speed up the training

but also boost the denoising performance that benefit the CNN learning. Figure 5(c) shows the result by the fast image deconvolution method FID-HL using Hyper-Laplacian priors, it is also effective and retains some details. Figure 5(d) is the result of the nonlocal image restoration method NLTV that reduces blocking artifacts. Figure 5(e) shows the result by the nonlocal gradient sparsity regularization method, which can balance preserving edges and retaining details. Figure 4(f) shows the recovered image of our proposed method that effectively alleviated block effects. Obviously, the proposed method can obtains the satisfied recovery result similar to that of the CNN method but does not need the high-performance hardware configuration required by the CNN algorithm.

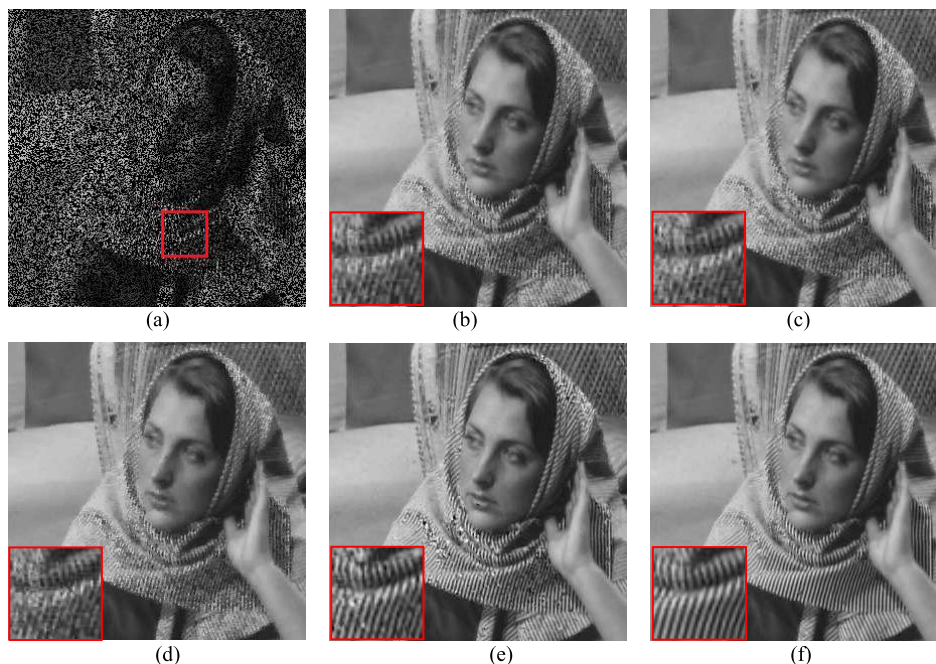


FIGURE 6. Comparison for image inpainting methods on image Barbara with the data ratio $r = 0.4$: (a) Masked image; (b) TwIST [13], PSNR = 25.39dB; (c) SALSA [16], PSNR = 25.62dB; (d) TVAL3 [5], PSNR = 25.83dB; (e) NGS [23], PSNR = 29.73dB; (f) Proposed, PSNR = 30.21dB.

TABLE 3. Image inpainting results of compared methods in PSNR(dB).

Method	r	Images (#)								
		1	2	3	4	5	6	7	8	9
TwIST	0.2	27.43	23.73	21.70	25.84	24.02	25.02	26.32	25.36	24.62
SALSA		28.68	23.93	22.69	26.52	24.36	25.92	27.61	25.74	24.93
TVAL3		29.23	24.07	23.28	26.97	24.67	26.52	27.93	26.12	25.47
NGS		30.79	24.68	23.86	27.98	25.12	27.54	30.59	26.54	25.92
Proposed		31.04	24.96	24.13	28.31	25.71	27.86	31.12	26.96	26.31
TwIST	0.4	30.99	25.39	25.08	29.33	25.51	28.56	30.53	30.33	29.11
SALSA		32.27	25.62	25.71	29.90	25.74	29.27	32.22	30.83	30.30
TVAL3		32.65	25.83	26.20	29.96	26.22	29.45	32.30	31.21	30.52
NGS		34.49	29.73	27.50	31.66	28.08	31.05	35.70	33.23	31.46
Proposed		35.02	30.21	27.94	31.97	28.89	31.46	35.92	33.61	31.74
TwIST	0.8	38.81	31.20	32.40	36.13	34.30	35.90	38.82	38.23	35.51
SALSA		40.06	31.69	32.66	36.21	34.61	36.57	40.36	38.94	35.96
TVAL3		40.46	31.87	33.17	36.75	34.84	36.96	40.81	39.03	36.32
NGS		42.28	40.36	34.94	38.46	35.92	38.81	43.92	41.82	36.87
Proposed		42.61	40.67	35.42	39.17	36.43	39.14	44.33	42.13	37.41

Denosing results of all test images are list in Table 2. Here, σ_n denotes the noise level with three different degrees 10, 20, 50. We can see that FID-HL and NLTV show the similar performance with the objective evaluation PSNR. Our proposed method using the nonlocal spatial gradient information is similar with the NGS but shows better performance. The improvement is using the L_0 -norm image smoothing preprocessing to get the accuracy and efficiency of block matching for similar patches clustering. Compared with the DnCNN method, the proposed method achieves comparable results when the noise level is low, and the DnCNN method shows better recovery performance when the image is severely degraded. It can also be observed that as the degree of degradation becomes larger, the difference

in recovery performance becomes smaller. This is due to the limited information available.

2) IMAGE INPAINTING

In image inpainting, the data ratio r varies from 0.2 to 0.8. The comparison methods including TwIST [13], SALSA [16], TVAL3 [5] and NGS [23] are all state-of-the-art methods and the recovered results on image *Barbara* are shown in Figure 6. Figure 6(a) is the masked image with the data ratio $r = 0.4$. Figure 6(b) shows the result of the TwIST by the two-step iterative shrinkage thresholding algorithms, which also apply the weighted L_p -norm in image restoration. Figure 6(c) shows the result of the SALSA (split augmented Lagrangian shrinkage algorithm), which uses the L_2 -norm

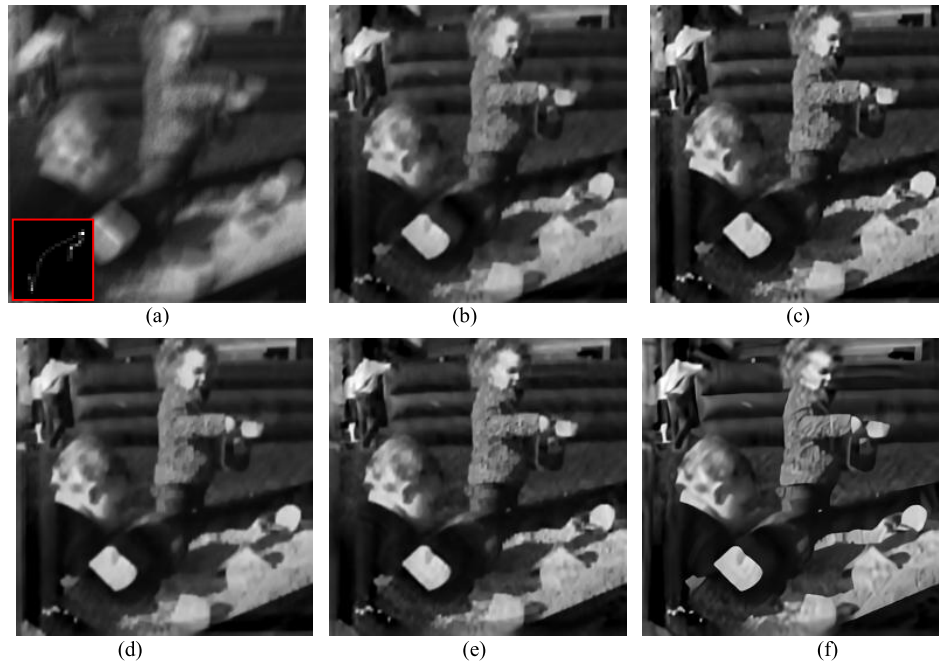


FIGURE 7. Comparison for image deblurring methods on image *Children* with the random motion blur:(a) Blurred image; (b) TVAL3 [5], PSNR = 18.89dB;(c) FID-HL [6], PSNR = 19.27dB;(d) LINC [10], PSNR = 19.23dB;(e) NGS [23], PSNR = 20.46dB;(f) Proposed method, PSNR = 20.87dB.

TABLE 4. Image deblurring results of comparison methods in PSNR(dB).

Method	H	Images (#)								
		1	2	3	4	5	6	7	8	9
TVAL3	27×27	20.52	19.42	17.96	18.48	18.03	18.89	20.21	20.16	18.71
FID-HL		20.94	19.81	18.43	18.67	18.39	19.27	20.66	20.63	19.13
LINC		21.45	20.37	18.92	19.02	19.06	19.23	21.04	21.11	19.59
NGS		21.79	20.78	20.31	19.43	19.53	20.46	21.59	21.62	20.02
Proposed		22.04	21.65	20.82	19.75	19.96	20.87	21.94	22.04	20.38
TVAL3	19×19	25.47	24.36	22.07	24.21	23.37	23.53	26.53	26.33	23.16
FID-HL		26.29	24.82	22.52	24.53	24.16	25.26	26.92	26.79	23.52
LINC		26.75	25.43	22.89	24.91	24.78	25.45	27.33	27.15	24.03
NGS		27.36	25.91	23.34	25.47	25.52	26.03	27.86	27.62	24.42
Proposed		27.71	26.27	23.71	25.82	26.07	26.41	28.22	28.11	25.04

data-fidelity term and a nonsmooth regularizer based on total variation. Figure 6(d) recovered by TVAL3 shows the similar visual effects with Figure 6(c). Figure 6(e) apply the nonlocal gradient sparsity regularization and preserves more details. Our result is shown in Figure 6(f), from which we can see that the proposed method has better performance than other methods. The most obvious comparison is reflected in the enlarged region of Barbara's scarf, marked as the red block. It contains lots of details and is usually used as a region of interest for comparison of recovery results.

The results of the restored image data PSNR with $r = 0.2$, $r = 0.4$ and $r = 0.8$ are listed in Table 3. It can be seen that images with less details get better results, such as *House* and *Lena*. This is because the more scattered pixel details makes the image more complicated and harder to recover. In the recovery process, they are easier to be treated as false edges that lead to block effects.

3) IMAGE DEBLURRING

In image deblurring, we choose the random motion blur and compare with TVAL3 [5], FID-HL [6], LINC [10] and NGS [23]. Typical experimental results on the image *Children* are shown in Figure 7. Figure 7(a) is the degrade image and the blur kernel with the size 27×27 is embedded in the lower left corner. Figure 7(b) is the result of TVAL3 algorithm that shows obvious block effects. Figure 7(c) shows the result of the fast image deconvolution method FID-HL that also uses hyper-Laplacian priors and alleviates block effects. Figure 7(d) is the result of linear estimator with neighborhood patch clustering (LINC) [10] algorithm that uses Gaussian Mixture Models (GMM) with spatially constrained patch clustering. Figure 7(e) shows the result of the NGS algorithm that applies nonlocal gradient sparsity regularization and patch-based adaptive spatial constraint. Compared with Figure 7(e), our method improves the strategy of selecting

Algorithm 1 Image Restoration Method With Patch-Based Nonlocal Adaptive Gradient Regularization

Input: a degraded image \mathbf{y} and the matrix of degradation kernel H

• Initialization: $\mathbf{w} = \mathbf{y}$, $\gamma^h = \gamma^v = 0$.

Laplacian parameter p is fixed by the statistic from the natural image gradient distribution;

Preprocessing with image smoothed by the L_0 -norm and getting the image \mathbf{x}^0 ;

Calculating the expectation m_i and variance σ_i according to the Eq. (6).

• Iteration:

for $k = 1, 2, \dots, K$

— for each exemplar patch (\mathbf{x}_i^0) do

* Collecting KNN patches S_i in the neighbourhood of \mathbf{x}_i^0 with the l_2 -norm distance in Eq.(5).

* Calculating the expectation m_i and variance σ_i according to the Eq. (4).

* Solve \mathbf{x} according to the Eq.(14);

* Solve \mathbf{w}^h -problem according to the Eq.(16);

* Solve \mathbf{w}^v -problem according to the Eq.(17);

— end for

Update auxiliary multipliers γ^h and γ^v ,
 $\|\mathbf{x}^k - \mathbf{x}^{k+1}\| / \|\mathbf{x}^{k+1}\| \leq 1 \times 10^{-3}$.

end for

Output: Obtain the restored image $\hat{\mathbf{x}}^{(K+1)}$

similar regions, which is to cluster similar patches from the L_0 -norm smoothed image and alleviates block effects and preserves image edges, as shown in Figure 7(f). Since the visual differences are not obvious, we also choose the smaller kernel 19×19 and list data results in the Table 4.

V. CONCLUSION

In this paper, a patch-based adaptive nonlocal gradient regularization method is proposed for image restoration in sensor networks. In order to make full use of image priors, it applies the hyper-Laplacian prior to formulate the gradient distribution of the statistics of natural images, and explores the patch-based nonlocal gradient prior to regularize the nonlocal self-similarity of similar image patches. Especially, the L_0 -norm smoothing image is innovatively used as the preprocessed image to improve the accuracy of clustering the similar image patches. For spatial variant constraints, adaptive weights are learning from the expectation and variance of a set of clustered nonlocal self-similarity patches to adjust weights for sparse gradient distribution at each pixel adaptively. Experimental results show that the proposed method has better performance in alleviating block effects and preserving image details.

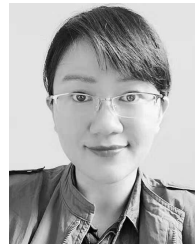
ACKNOWLEDGMENT

The author would like to thank reviewers for helping him to improve this article.

REFERENCES

- [1] Q. Liang, X. Cheng, S. C. Huang, and D. Chen, "Opportunistic sensing in wireless sensor networks: Theory and application," *IEEE Trans. Comput.*, vol. 63, no. 8, pp. 2002–2010, Aug. 2014.
- [2] J. Liang, X. Yu, and H. Li, "Collaborative energy-efficient moving in Internet of Things: Genetic fuzzy tree versus neural networks," *IEEE Internet Things J.*, vol. 6, no. 4, pp. 6070–6078, Aug. 2019.
- [3] K. Zhang, W. Zuo, Y. Chen, D. Meng, and L. Zhang, "Beyond a Gaussian Denoiser: Residual learning of deep CNN for image denoising," *IEEE Trans. Image Process.*, vol. 26, no. 7, pp. 3142–3155, Jul. 2017.
- [4] J. Liang and F. Zhu, "Soil moisture retrieval from UWB sensor data by leveraging fuzzy logic," *IEEE Access*, vol. 6, pp. 29846–29857, 2018.
- [5] C. Li, W. Y. Wotao, and Y. Zhang. (2013). *TVAL3: TV Minimization by Augmented Lagrangian and Alternating Direction Algorithms*. [Online]. Available: <http://www.caam.rice.edu/optimization/L1/TVAL3/>
- [6] D. Krishnan and R. Fergus, "Fast image deconvolution using hyper-Laplacian priors," in *Proc. 23rd Annu. Conf. Neural Inf. Process. Syst.*, Vancouver, BC, Canada, Dec. 2009, pp. 7–10.
- [7] J. Cheng, Y. Gao, and B. Guo, "Image restoration using spatially variant hyper-Laplacian prior," *Signal Image Video Process.*, vol. 13, pp. 155–162, Feb. 2018.
- [8] M. Shi and L. Feng, "Plug-and-play prior based on Gaussian mixture model learning for image restoration in sensor network," *IEEE Access*, vol. 6, pp. 78113–78122, 2018.
- [9] C. Bouman and K. Sauer, "A generalized Gaussian image model for edge-preserving MAP estimation," *IEEE Trans. Image Process.*, vol. 2, no. 3, pp. 296–310, Jul. 1993.
- [10] M. Niknejad, H. Rabbani, and M. Babaie-Zadeh, "Image restoration using Gaussian mixture models with spatially constrained patch clustering," *IEEE Trans. Image Process.*, vol. 24, no. 11, pp. 3624–3636, Nov. 2015.
- [11] Y. Rivenson, Y. Zhang, and H. Gunaydin, "Phase recovery and holographic image reconstruction using deep learning in neural networks," *Light. Sci. Appl.*, vol. 7, no. 141, pp. 1–9, 2017.
- [12] A. Buades, B. Coll, and J. Morel, "A non-local algorithm for image denoising," in *Proc. IEEE Comput. Soc. Conf. Pattern Recognit. (CVPR)*, San Diego, CA, USA, vol. 2, Jun. 2005, pp. 60–65.
- [13] J. M. Bioucas-Dias and M. A. T. Figueiredo, "A new TwIST: Two-step iterative shrinkage/thresholding algorithms for image restoration," *IEEE Trans. Image Process.*, vol. 16, no. 12, pp. 2992–3004, Dec. 2007.
- [14] J. Liang and C. N. Mao, "Distributed compressive sensing in heterogeneous sensor network," *Signal Process.*, vol. 126, pp. 96–102, Sep. 2016.
- [15] R. Rubinfeld, T. Peleg, and M. Elad, "Analysis K-SVD: A dictionary-learning algorithm for the analysis sparse model," *IEEE Trans. Signal Process.*, vol. 61, no. 3, pp. 661–677, Feb. 2013.
- [16] X. Yu and J. Liang, "Genetic fuzzy tree based node moving strategy of target tracking in multimodal wireless sensor network," *IEEE Access*, vol. 6, pp. 25764–25772, 2018.
- [17] M. Wei, F. Xing, and Z. You, "A real-time detection and positioning method for small and weak targets using a 1D morphology-based approach in 2D images," *Light Sci. Appl.*, vol. 7, no. 18006, pp. 1–9, 2018.
- [18] Y. Zhang, M. Ouyang, and A. Ray, "Computational cytometer based on magnetically modulated coherent imaging and deep learning," *Light Sci. Appl.*, vol. 8, no. 91, pp. 1–9, 2019.
- [19] T. S. Cho, N. Joshi, C. L. Zitnick, S. B. Kang, R. Szeliski, and W. T. Freeman, "A content-aware image prior," in *Proc. IEEE Comput. Soc. Conf. Pattern Recognit.*, San Francisco, CA, USA, Jun. 2010, pp. 169–176.
- [20] X. Zhang, M. Burger, X. Bresson, and S. Osher, "Bregmanized nonlocal regularization for deconvolution and sparse reconstruction," *SIAM J. Imag. Sci.*, vol. 3, no. 3, pp. 253–276, 2010.
- [21] K. Dabov, A. Foi, V. Katkovnik, and K. Egiazarian, "Image denoising by sparse 3-D transform-domain collaborative filtering," *IEEE Trans. Image Process.*, vol. 16, no. 8, pp. 2080–2095, Aug. 2007.
- [22] W. Dong, L. Zhang, and G. Shi, "Nonlocally centralized sparse representation for image restoration," *IEEE Trans. Image Process.*, vol. 22, no. 4, pp. 1618–1628, Apr. 2013.
- [23] H. Liu, R. Xiong, and X. Zhang, "Non-local gradient sparsity regularization for image restoration," *IEEE Trans. Circuits Syst. Video Technol.*, vol. 27, no. 9, pp. 1909–1921, Sep. 2017.
- [24] Z. Daniel and Y. Weiss, "From learning models of natural image patches to whole image restoration," in *Proc. Int. Conf. Comput. Vis.*, Barcelona, Spain, Nov. 2011, pp. 479–486.
- [25] V. Pappayan and M. Elad, "Multi-scale patch-based image restoration," *IEEE Trans. Image Process.*, vol. 25, no. 1, pp. 249–261, Jan. 2016.

- [26] M. Shi, T. Han, and S. Liu, "Total variation image restoration using hyper-Laplacian prior with overlapping group sparsity," *Signal Process.*, vol. 126, pp. 65–76, Sep. 2016.
- [27] D. C. Alban, S. Parameswaran, and T. Q. Nguyen, "Image restoration with generalized Gaussian mixture model patch priors," *SIAM J. Imag. Sci.*, vol. 11, no. 4, pp. 2568–2609, 2018.
- [28] K. Ni and Y. Wu, "Adaptive patched L_0 gradient minimisation model applied on image smoothing," *IET Image Process.*, vol. 12, no. 10, pp. 1892–1902, Oct. 2018.
- [29] J. Qin, R. M. Silver, and B. M. Barnes, "Deep subwavelength nanometric image reconstruction using Fourier domain optical normalization," *Light Sci. Appl.*, vol. 5, Feb. 2016, Art. no. e16038.
- [30] A. M. Teodoro, J. M. Bioucas-Dias, and M. A. T. Figueiredo, "Image restoration and reconstruction using variable splitting and class-adapted image priors," in *Proc. IEEE Int. Conf. Image Process. (ICIP)*, Phoenix, AZ, USA, Sep. 2016, pp. 3518–3522.
- [31] X. Pang, S. Zhang, and J. Gu, "Improved L_0 gradient minimization with L_1 fidelity for image smoothing," *PLoS ONE*, vol. 10, no. 9, pp. 1–10, 2015.
- [32] L. Xu, S. Zheng, and J. Jia, "Unnatural L_0 sparse representation for natural image deblurring," in *Proc. IEEE Conf. Comput. Vis. Pattern Recognit.*, Portland, OR, USA, Jun. 2013, pp. 1107–1114.
- [33] J. Pan, Z. Hu, Z. Su, and M. Yang, " L_0 -regularized intensity and gradient prior for deblurring text images and beyond," *IEEE Trans. Pattern Anal. Mach. Intell.*, vol. 39, no. 2, pp. 342–355, Feb. 2017.
- [34] M. Zontak and M. Irani, "Internal statistics of a single natural image," in *Proc. IEEE Conf. Comput. Vis. Pattern Recognit.*, Colorado Springs, CO, USA, Jun. 2011, pp. 977–984.
- [35] R. W. Liu, L. Shi, W. Huang, J. Xu, S. C. Yu, and D. Wang, "Generalized total variation-based MRI Rician denoising model with spatially adaptive regularization parameters," *Magn. Reson. Imag.*, vol. 32, no. 6, pp. 702–720, Jul. 2014.
- [36] W. Zuo, D. Meng, L. Zhang, X. Feng, and D. Zhang, "A generalized iterated shrinkage algorithm for non-convex sparse coding," in *Proc. IEEE Int. Conf. Comput. Vis.*, Sydney, NSW, Australia, Dec. 2013, pp. 217–224.
- [37] X. Liu, M. Jia, X. Zhang, and W. Lu, "A novel multichannel Internet of things based on dynamic spectrum sharing in 5G communication," *IEEE Internet Things J.*, vol. 6, no. 4, pp. 5962–5970, Aug. 2019.



MINGZHU SHI received the B.S. degree from Xi'an Technological University, China, in 2008, and the Ph.D. degree in Beijing Institute of Technology, China, in 2014. She is currently working with Tianjin Normal University. Her current interests include image processing, machine learning, and pattern recognition.

• • •